Upscattering of ultracold neutrons from gases

S. J. Seestrom,[1] E. R. Adamek,[2] D. Barlow,[1] L. J. Broussard,[1] N. B. Callahan,[2] S. M. Clayton,[1] C. Cude-Woods,[2] S. Currie,[1] E. B. Dees,[4] W. Fox,[2] P. Geltenbort,[4] K. P. Hickerson,[5] A. T. Holley,[2] C.-Y. Liu,[2] M. Makela,[1] J. Medina,[1] D. J. Morley,[1] C. L. Morris,[1] J. Ramsey,[1] A. Roberts,[1] D. J. Salvat,[1,2] A. Saunders,[1] E. I. Sharapov,[6] S. K. L. Sjue,[1] B. A. Slaughter,[2] B. VornDick,[3] P. L. Walstrom,[1] Z. Wang,[1] T. L. Womack,[1] A. R. Young,[1,3] and B. A. Zeck[3]
(UCNτ Collaboration)
[1]*Los Alamos National Laboratory, Los Alamos, New Mexico 87545, USA*
[2]*Indiana University, Bloomington, Indiana 47405, USA*
[3]*North Carolina State University, Raleigh, North Carolina 27695, USA*
[4]*Institut Laue Langevin, 38042 Grenoble, France*
[5]*University of California Los Angeles, Los Angeles, California 90095, USA*
[6]*Joint Institute for Nuclear Research, 141980, Dubna, Russia*
(Received 4 February 2015; revised manuscript received 8 September 2015; published 14 December 2015)

We present measurements of the upscattering cross sections of ultracold neutrons (UCNs) from room-temperature hydrogen, deuterium, neon, argon, xenon, C_4H_{10}, CF_4, and air. The values of these cross sections are important for estimating the loss rate of trapped neutrons due to residual gas and are therefore of importance for neutron lifetime measurements using UCNs. Cross sections were obtained from a combined analysis of the UCN attenuation in a gas cell and direct measurement of the neutrons upscattered in the cell. The effects of the UCN velocity and path-length distributions were accounted for using a Monte Carlo transport code. Results are compared with measurements at higher neutron energy as well as with calculations.

DOI: 10.1103/PhysRevC.92.065501 PACS number(s): 25.40.Fq, 25.40.Kv, 28.20.Cz, 28.20.Ka

I. INTRODUCTION

The UCNτ Collaboration has built a large volume 0.6 m^3 magnetogravitational trap that will be used to measure the lifetime of the free neutron [1]. In order to investigate possible systematic effects that could impact our measurement of the neutron lifetime, the Collaboration is using the Los Alamos Neutron Science Center (LANSCE) ultracold neutron source [2]. One source of systematic errors comes from absorption and upscattering due to residual gas. Here we report measurements of the cross section for upscattering of ultracold neutrons (UCNs) by potential residual gases that could be found within the UCNτ apparatus. Residual gas in the trap can absorb or upscatter the stored UCNs to cold or thermal energies, thus introducing a potential source of UCN loss in the experiment. Recent neutron lifetime measurements using material bottles have corrected for this effect. Arzumanov and co-workers [3,4] introduce a 0.2-s uncertainty (but no correction) in their determination of τ_n for a trap pressure of 1×10^{-6}–5×10^{-6} torr. Pichlmaier *et al.* [5] introduce various corrections depending on the observed vacuum pressure and composition, ranging from 0.7 to 1.4 s. The larger corrections were due to the outgassing of Fomblin oil that was observed with a mass spectrometer and fine pressure gauge. Thereafter the pressure was stable at 3.8×10^{-6} torr, and the dominant residual gas that can cause upscattering was water vapor. All corrections quoted a 0.4-s uncertainty stated to be due to the location of the measurement devices. Serebrov *et al.* [6] corrected for this effect by measuring the storage time of the trap at two pressures $P = 3.8 \times 10^{-6}$ and $P = 6 \times 10^{-4}$ torr, and the loss rate $\tau_g^{-1} \propto P$ was determined by the difference between these two measurements, giving a 0.4 ± 0.024 correction to the measurement of the neutron lifetime. However, the size of the correction and its uncertainty are expected to depend strongly on the species of residual gas and stability of vacuum conditions. These various approaches motivate the measurements shown here as they can be used to place limits on the amount of these gases that can be tolerated in our system to meet the goal of a measurement with sub-1-s accuracy.

The thermal and cold neutron total cross sections for scattering from gases have been the subject of earlier investigations for molecular [7,8] and noble gases [9] and are found in agreement with theoretical expectations. Recently the ultracold neutron scattering cross section for deuterium gas was measured [10] for better understanding of the mechanism of ultracold neutron production in gases, liquids, and solids. Figure 1 presents a spectrum from a residual gas analyzer connected to the vacuum system of our neutron trap. The dominant contaminants in our system were water vapor (including both H_2O and OH), N_2, and O_2. Hydrocarbon gases that are frequently used as detector gases are potential contaminants. For the measurements presented here, we chose a set of gases that included potential contaminants and spanned a range of mass. The molecular gases are of interest, both as potential contaminants and to test theoretical predictions [11–13]. We further chose a set of noble gases whose cross sections should be straightforward to calculate and therefore could be used as a test of our experimental method.

In subsequent sections we describe our UCN measurements.

II. DESCRIPTION OF THE EXPERIMENT

The experimental configuration is shown in Fig. 2. UCNs enter from the UCN source [2] (left). The experimental setup contained three detectors: a ^{3}He-filled multiwire proportional chamber to provide a relative UCN fluence monitor [14] (*M* in Fig. 2), a commercial high purity germanium γ-ray detector

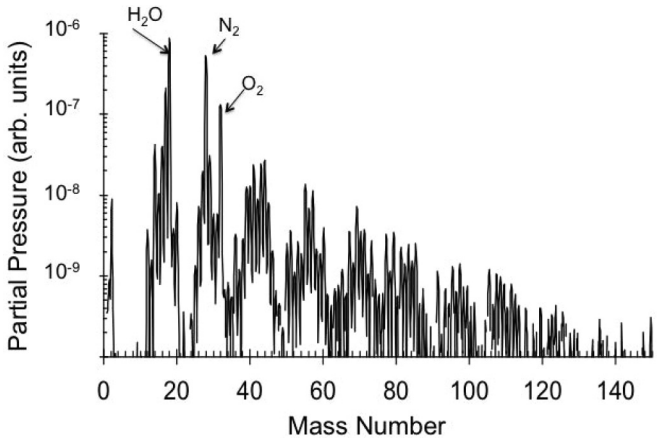

FIG. 1. RGA spectrum. The main contaminants appear at masses of 17, 18, 28, and 32 corresponding to OH, H_2O, N_2, and O_2. Peaks at large masses are likely Ar (mass 40) and heavy hydrocarbons.

(HPGe in Fig. 2), and a ^{3}He-filled drift tube neutron detector (HE in Fig. 2). The UCNs pass through a GV (open for these measurements) and a 6-T solenoidal polarizing magnet (*P*). A curved electropolished stainless-steel guide elbow (7.6 cm in diameter with a 30.5-cm bending radius) leads downward to a cylindrical gas cell (*G*). The vertical distance from the center of the main beamline guide to the entrance of the gas cell is 1 m. The gas cell is 7.6-cm long $\times$ 7.6 cm in diameter with a 0.127-mm aluminum window separating the cell from the guide system. This cell was developed as a detector for the UCN, and it was lined with a thin layer of ^{10}B [15]. Here, instead of being used as a detector, the cell was used as a neutron-absorbing and scattering cell to hold the gases to be studied (the target). The cell was filled with different gas species, and each was measured over a range of pressures $0 < P < 1000$ mbars. The temperature was 25 ± 1 °C over the course of the experiment.

In the cell, neutrons that reach the wall without being upscattered have a high probability (near 100%) of being

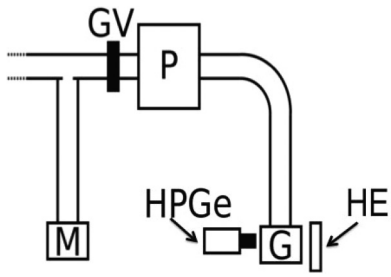

FIG. 2. Schematic of the experimental setup (not to scale). The curved guide is 7.6-cm diameter electropolished stainless steel with a 30.5-cm bending radius. The vertical guide is 7.6-cm electropolished stainless steel. The total distance from the center of the beam height to the cell window is 1 m. *M* is a ^{3}He-filled multiwire proportional chamber permanently installed at the UCN source, used to monitor the UCN production. *G* is the boron-lined gas cell. The HPGe detector is used to detect γ rays from capture on the boron layer. He is the ^{3}He-filled drift tube used to detect upscattered neutrons from the cell. GV is a gate valve, and *P* is a polarizing magnet.

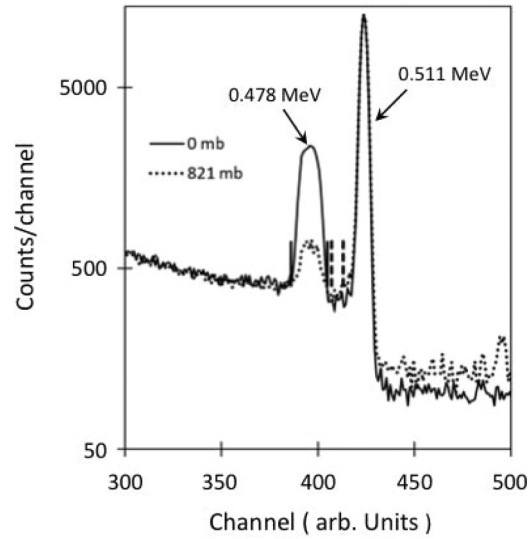

FIG. 3. γ-ray spectra measured for two different pressures of C_4H_{10} in the cell. The dotted line corresponds to a gas target cell pressure of 821 mbars; the solid line is for an empty target. The peak labeled 0.478 MeV is from the decay of ^{7}Li. The peak labeled 0.511 MeV is from pair production by room background. The larger counting rates above the 0.511-MeV peak are due to Compton γ-ray events induced by captured neutrons in the detector or surrounding materials.

captured via $^{10}\mathrm{B}\,(n,\alpha)\,^7\mathrm{Li}^*$. This reaction results in a prompt 0.478-MeV decay γ ray with a probability of 94%. The detector HPGe is used to detect this γ ray; a spectrum is shown in Fig. 3. The attenuation of the ^{10}B capture signal by the gas is readily apparent. Upscattered neutrons can also interact with material, generating γ rays that subsequently generate a signal in this detector through Compton scattering; this results in the increased background visible above the 0.511-MeV peak in the measurement at a pressure of 821 mbars.

Upscattered UCNs were directly detected in detector HE. This detector is a 5-cm diameter 31.8-cm drift tube filled with 1.8 bars of ^{3}He. Spectra from this neutron detector are shown in Fig. 4. The counts at low pulse height in Fig. 4 are due to neutrons that capture near the walls of the drift tube for which only part of the full energy contained in the proton and triton from ^{3}He plus a neutron is detected.

For these measurements, the source was operated in a pulsed mode with a pulse chain occurring every 5 s (see Ref. [2] for a detailed description of the source operation). The UCNs are extracted from the source through the bulk shielding using a transfer line with a chicane into the very low background experimental area. This results in many bounces as the UCNs pass through the guide and thus provides very effective filtering of the neutron velocity spectrum. The neutron potential of the stainless-steel guides (189 neV) corresponds to a maximum 609-cm s velocity for neutrons incident normally. There are few neutrons above this energy. Spectra were calculated using the Monte Carlo code "UCN" [16], yielding an average velocity at a beam height outside the bulk shield of 486 cm s. The benchmark simulations presented in Ref. [2] have established the validity of this code. Calculated spectra for neutrons inside the solid $^2\mathrm{H}\,(\mathrm{SD}_2)$ volume in which they are produced,

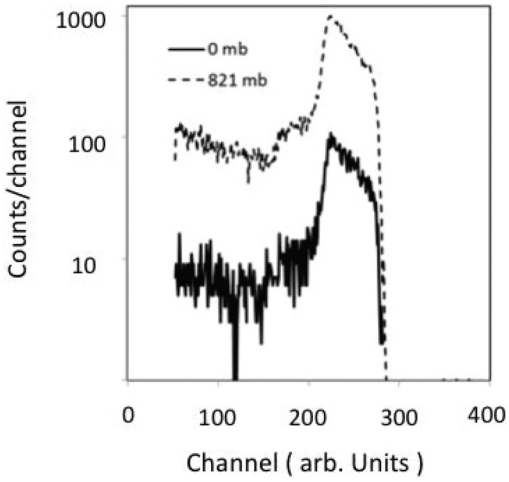

FIG. 4. Spectra from the upscattered neutron detector for two different pressures of C_4H_{10} in the cell. The finite peak measured with the empty cell is due to the ambient thermal neutron background. The peak near channel 200 is when the energy from both the proton and triton from neutron capture on ^{3}He is deposited in the gas; the lower-energy counts correspond to the event where the energy is partially deposited on the wall.

neutrons at beam height, and neutrons after dropping the 1 m into the gas cell are plotted in Fig. 5. Data were acquired for 500 s at each pressure, and the monitor detector (M) was used to normalize each measurement. No appreciable background is observed in this detector, and the monitoring rate is not affected by the presence of gas in the cell. The UCN source was stable within the statistical sensitivity of these measurements.

A. Data analysis

1. Model

Each detector measured a quantity sensitive to the upscattering cross section: the HPGe was primarily sensitive to the UCN

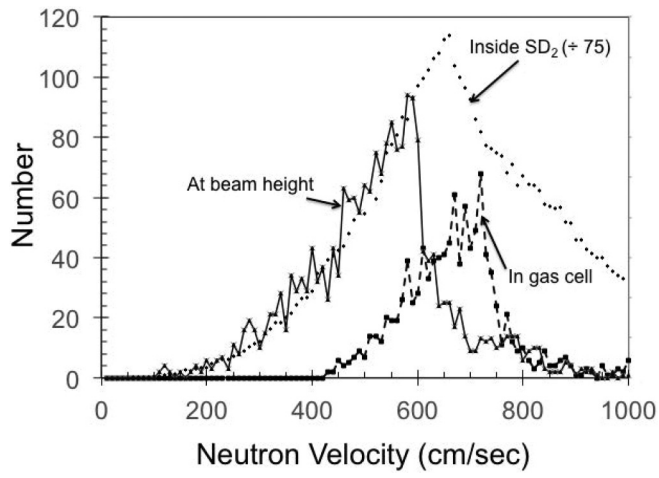

FIG. 5. Spectra showing the number of neutrons as a function of neutron velocity generated using the Monte Carlo code UCN for neutrons inside the source solid $^2H(SD_2)$ (circles) for neutrons at the beam height near the gas cell (solid line) and inside the gas cell (dashed line).

that did *not* interact in the gas, whereas the neutron detector HE was sensitive only to those UCNs that *did* upscatter in the gas.

The yield of upscattered neutrons measured in the upscattered neutron detector was normalized to the counts in a detector (M) located near the gate valve ($N_{\rm GV}$). Background-subtracted yields were calculated by subtracting the yield obtained combining target empty runs that were taken just before and just after the gas sample measurements. In the hypothetical case of a well-defined path length and single neutron energy, yields can be connected to upscattering cross section via

$$Y_{\rm exp}(P) = \frac{\sigma_{\rm up}}{\sigma_T} F\Omega\varepsilon[1 - \exp(-\rho_{\rm volume}\sigma_T l)]. \quad (1)$$

Here l is the cell thickness, Ω is the solid angle of the neutron detector, ε is the detection efficiency for the neutron detector HE, and F is the neutron fluence φ_n per count $N_{\rm GV}$ in the beam monitor detector M,

$$F = \frac{\varphi_{\rm neutron}}{N_{\rm GV}}, \quad (2)$$

and

$$\sigma_T = \sigma_{\rm absorption} + \sigma_{\rm up}, \quad (3)$$

where $\rho_{\rm volume}$ is the number density of the target gas for a gas temperature of 25 °C given by

$$\rho_{\rm volume} = 2.43 \times 10^{16} \times P({\rm mbar})\left(\frac{\rm atoms}{\rm cm^3\ mbar}\right). \quad (4)$$

The detection efficiency ε includes the efficiency of the neutron detector HE itself and the attenuation due to absorption of the upscattered neutrons in the stainless-steel wall of the gas cell and in the ^{10}B coating on the cell. All these factors depend on the energy of the upscattered neutrons. This energy was not measured and is expected to be different for each gas sample. The neutron detector data also require a normalization of the flux-solid angle product $F\Omega$.

The transmission ratio at pressure P is defined in terms of the yield of 478-keV γ rays $Y_\gamma(P)$ and can be written as follows:

$$T_n(P) = \frac{Y_\gamma(P)}{Y_\gamma(P=0)} = \frac{F\Omega_\gamma\varepsilon_\gamma[\exp(-\rho_{\rm vol}\sigma_T l)]}{F\Omega_\gamma\varepsilon_\gamma}$$
$$= \exp(-\rho_{\rm vol}\sigma_T l). \quad (5)$$

In this case there is no need to determine an efficiency or absolute neutron fluence normalization. For this reason, it is preferable to extract the upscattering cross section from this data if possible.

Because of the distribution of neutron energies and angles entering the cell, there is a range of different mean-free paths for UCNs within the cell. We have accounted for this using the results of the Monte Carlo transport program UCN [16], which has been benchmarked previously for the characterization of the LANSCE UCN source [2]. Ultimately, the quality of the description of the transmission ratio data at high pressures is a good validation of the simulation. In the simulation performed here, neutrons are transported from the solid deuterium source to the gas cell in a simplified geometry that accounts for the

velocity shift due to the SD_2 potential, the UCN transport through the guide system, and transmission into the gas cell window. In this simulation the ^{10}B-coated gas cell wall was taken to be 100% absorptive for the UCN. Neutrons in the volume of the gas cell are absorbed with a lifetime τ, which is a variable in the simulation. To a good approximation, both absorption and upscattering result in UCN lifetimes that are independent of velocity because for both processes the first-order cross sections are given by $\sigma_0 = \sigma(v)\,v$ where v is the UCN velocity, $\sigma(v)$ is the cross section, and σ_0 is a constant. The lifetime is related to the total cross section,

$$\tau = \frac{1}{\rho\sigma_T v}, \tag{6}$$

where ρ is the number density of the cell, given by Eq. (4), and σ_T is the total cross section.

The total cross section is the sum of the upscattering cross section and the absorption cross section. The absorption cross section is taken from the thermal neutron value in the NIST tables [17] and scaled to the appropriate neutron velocity using a $1/v$ dependence.

The average neutron velocity in the cell $\bar{v}$ and path length to the wall $\bar{l}$ were calculated from the Monte Carlo to be 660 cm s and 5.3 cm, respectively. The average neutron velocity is higher than that at the beam height because of the ∼1-m drop to the gas cell. From the number of neutrons interacting in the gas N_i and absorbing on the wall N_w, an average transmission $T_n(\tau) = N_w/(N_i + N_w)$ was calculated for a range of values for the lifetime τ. This is plotted as a function of the inverse lifetime in Fig. 6. Also shown (the dashed line in the figure) is a simple exponential obtained using $\bar{v}$ and $\bar{l}$ from the Monte Carlo. Although this describes the data well for long lifetimes, it fails for short lifetimes and larger attenuation because of the broad UCN spectrum incident upon the cell. To achieve a better description of the Monte Carlo results, we have fitted a

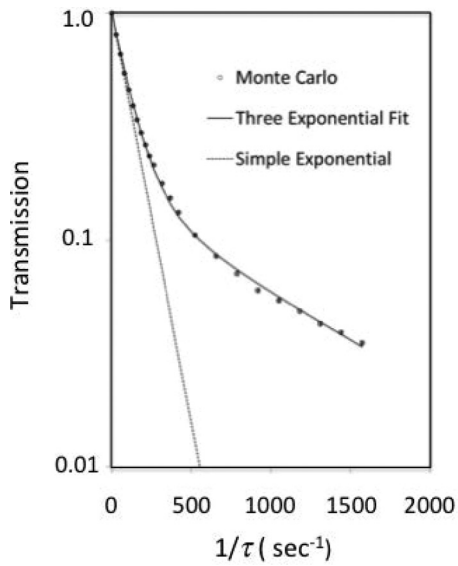

FIG. 6. Fits to the Monte Carlo data where the points are for different UCN lifetimes in the gas cell using a simple exponential (dotted line) and a triple exponential function (solid line).

three-exponential model to the transmission as shown by the solid line in Fig. 6,

$$T_n = a_1 e^{-(k_1/\tau)} + a_2 e^{-(k_2/\tau)} + a_3 e^{-(k_3/\tau)}. \tag{7}$$

Here the amplitudes $a_1 + a_2 + a_3 = 1$ and values of k_1,k_2, and k_3 (where $k = l/v$) were chosen to give a good fit to the Monte Carlo prediction of transmission. The use of the three values of l/v is similar to the practice in which a limited number of neutron groups are used to approximate a complex neutron spectrum in many Monte Carlo applications.

2. *Fitting*

The function in Eq. (7) can be used to fit the transmission ratio $T_n(P)$ defined in (5) (varying the upscattering cross section, and hence τ) measured with the HPGe γ detector as a function of pressure to extract a $\sigma_{\rm up}$. The total cross section σ_T is the sum of the upscattering cross section and the absorption cross section. The absorption cross section is taken from the thermal neutron value in the NIST tables [17] as described above.

The upscattered neutron yield $Y_{\rm exp}$ data can be fitted with the following related function:

$$Y_{\rm exp}(P) = \frac{\sigma_{\rm up}}{\sigma_T} F\Omega\varepsilon[1 - (a_1 e^{-k_1/\tau} + a_2 e^{-k_2/\tau} + a_3 e^{-k_3/\tau})]. \tag{8}$$

The lifetime τ is related to the pressure through Eqs. (4) and (6) with v determined to be the average UCN energy $\bar{v} = 660$ cm s.

The detection efficiency in detector HE is given by

$$\varepsilon = \varepsilon_{^3{\rm He}} T_B T_{ss}. \tag{9}$$

T_B is the transmission through the ^{10}B layer and T_{ss} is the transmission through the stainless-steel walls of the gas cell. The neutron detector efficiency as a function of neutron energy was taken from a calculation using the LANL MCNP code [18] that modeled the detector. The transmissions through the boron and stainless steel were calculated from the NIST thermal neutron cross-sectional tables [17], scaled to the expected upscattered energy using the expected $1/v$ dependence. For stainless steel, the atomic composition of 304 stainless steel was used to calculate a stainless-steel cross section from the atomic cross sections in the NIST table. The thickness of the stainless steel was fixed at the known value. The ^{10}B was applied by a sprayed on powder coating with thickness estimated [15] to be 1.5 ± 0.5 μm. We let the ^{10}B thickness be a variable parameter in our fits. Note that the upscattering cross sections extracted from the transmission ratio data are relatively insensitive to the ^{10}B thickness because it impacts only the contributions of the upscattered neutrons to the transmission data described below. UCN interacting with the ^{10}B are 100% absorbed for any reasonable values of the ^{10}B thickness, and therefore the effective target length is not impacted by the value of the ^{10}B thickness.

We must account for the contribution to the transmission ratio T_n from neutrons that upscatter and subsequently are captured in the ^{10}B layer as they exit the gas cell. To model this we added a term relating the number of upscattered neutrons

multiplied by $(1 - T_B)$, the probability that an upscattered neutron is captured in the ^{10}B layer. The resulting fitting function for the transmission ratio data is as follows:

$$T_n(P) = [a_1 e^{-k_1/\tau} + a_2 e^{-k_2/\tau} + a_3 e^{-k_3/\tau}] + (1 - T_B) \times \frac{\sigma_{\rm up}}{\sigma_T}[1 - (a_1 e^{-k_1/\tau} + a_2 e^{-k_2/\tau} + a_3 e^{-k_3/\tau})]. \quad (10)$$

The fitted parameters used to describe the transmission data are the upscattering cross sections and the thickness of the ^{10}B layer inside the gas cell. Hence, it is this datum alone that is used to determine the upscattering cross section. To describe the upscattering yield from the neutron detector, a value for the flux-solid angle must be fitted using the cross sections and ^{10}B thickness determined from the fits to the transmission data. As mentioned previously, the energy of the upscattered neutrons is required to determine both the neutron detector efficiency and the transmission through the ^{10}B and stainless steel. The theoretical calculations described in Sec. III provide a reasonable estimate for the outgoing energies for cold neutrons from upscattering from the noble gases H_2 and $^2H_2$ (D_2). For C_4H_{10}, CF_4, and air this energy was treated as a variable parameter. The upscattered energies are in the range of 25 meV (thermal) down to ∼1 meV (for the heaviest gas Xe). The overall detection efficiency (calculated for the best-fit ^{10}B layer thickness of 1.5μm), T_B, T_{ss}, and the ^{3}He detector efficiency as a function of energy are plotted in Fig. 7. The fitting procedure resulted in rather large upscattered energies for C_4H_{10}, CF_4, and air (25, 25, and 18 meV, respectively); a limit of 25 meV was imposed to avoid physically unreasonable values. It is likely that this suspiciously large value of v acts to account for some inadequacy in the model for the neutron yield at the gas pressures for which most neutrons are upscattered. This could include for example, the use of only three neutron groups to describe the UCN spectrum or a dependence of the solid angle of the detector HE on the location at which the upscattering occurs in the target.

Because of the additional uncertainties in extraction of upscattering cross sections from the direct upscattered neutron measurements, we have chosen to extract the cross sections from the transmission data only where possible. This is true for the polyatomic gases, which exhibit a significant decrease in transmission as a function of pressure. For these gases, we simultaneously fitted all transmission data, varying only the individual upscattering cross sections and the ^{10}B layer thickness [which determines T_B in Eqs. (9) and (10)]. For these gases the $\frac{\chi^2}{\rm DOF} \sim 1$ where DOF represents degree of freedom. We then obtained the best description possible for the direct neutron upscattering data by varying only the flux solid angle product $F\Omega$ and the upscattered energy for C_4H_{10}, CF_4, and air as a consistency check. In this case, $\frac{\chi^2}{\rm DOF} \sim 20$. In contrast, it is the direct neutron upscattering data that are most sensitive to the upscattering cross sections for Ne and Ar because those cross sections are quite small (and hence result in very little attenuation). For Xe, the transmission data are dominated by the very large absorption cross section. Therefore, for all three of these noble-gas samples we fitted each upscattering cross section simultaneously to the transmission and upscattering data while keeping $F\Omega$ and the ^{10}B thickness fixed at the

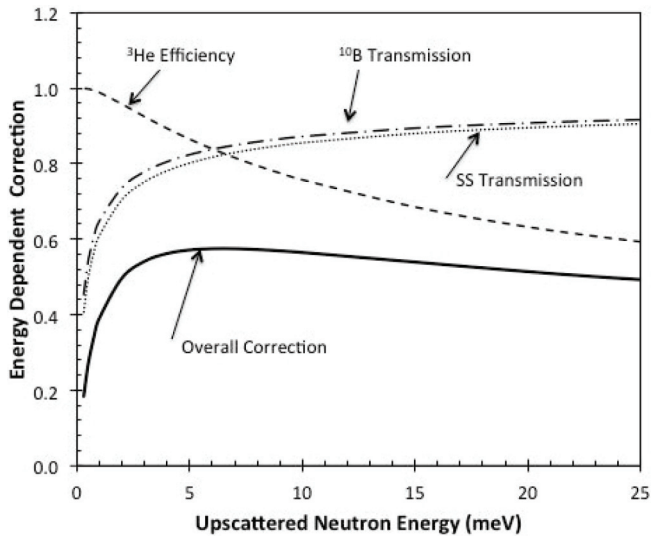

FIG. 7. The energy-dependent correction (solid line) ε, which is the product of the efficiency of the ^{3}He detector (dashed line), the transmission through the boron layer in the gas cell (dot-dashed line), and the transmission through the stainless steel of the gas cell (dotted line) as a function of upscattered neutron energy.

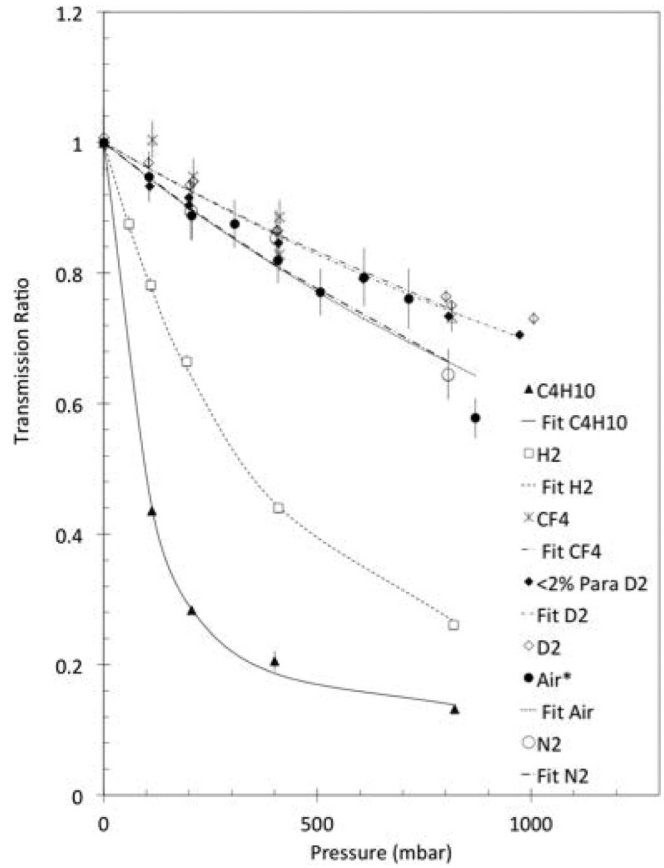

FIG. 8. Transmission ratio data and fits for the polyatomic gas samples H_2, $^2H_2$(D_2), C_4H_{10}, CF_4, N_2, and air. The transmission ratio is calculated by taking the ratio of the 0.478-MeV γ line with and without gas in the measurement cell.

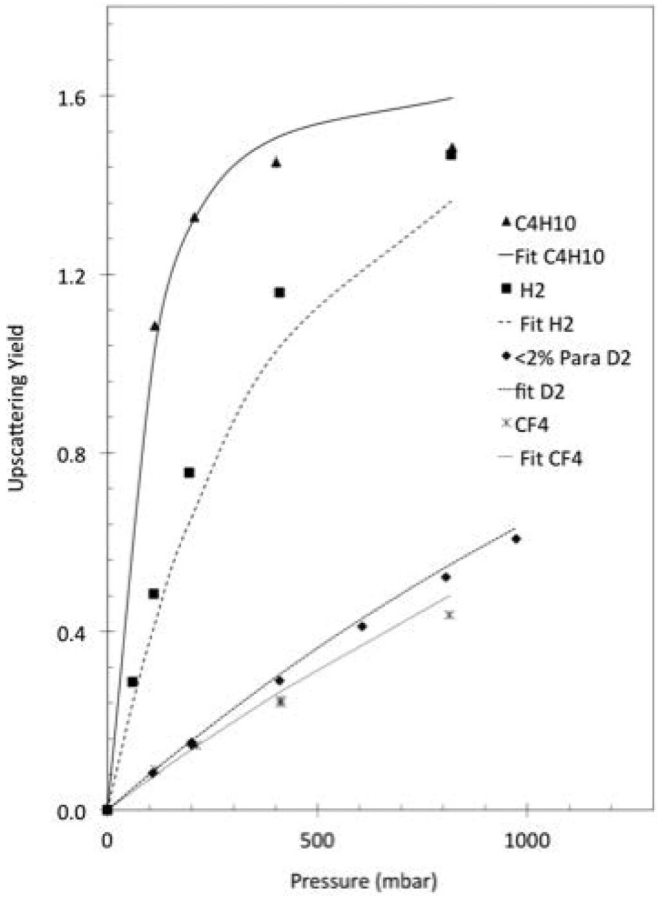

FIG. 9. Upscattering yields from the ^{3}He upscattered neutron detector and fits for the polyatomic gas samples H_2, $^2H_2(D_2)$, C_4H_{10}, and CF_4.

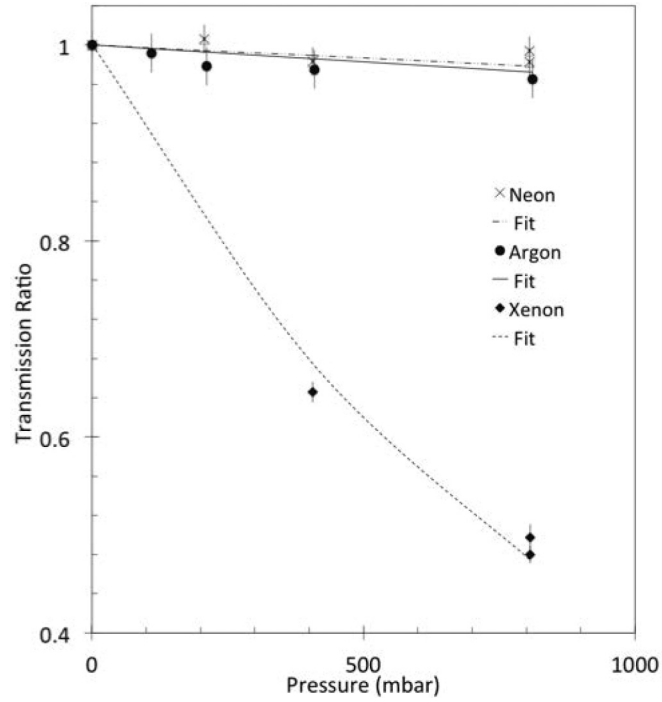

FIG. 10. Transmission ratio data and fits for the noble-gas samples.

best-fit values previously determined for the polyatomic gases. For these fits, $\frac{\chi^2}{\mathrm{DOF}} \leqslant 1$.

The data and resulting fits are shown in Figs. 8–11. The extracted upscattering cross sections are listed in Table I. The uncertainties in the table include the statistical uncertainties and the uncertainty due to the fitting procedure. We performed an initial estimate of the fitting uncertainties by varying the cross section to change the χ^2 by 1 and then scaled the resulting cross-sectional change by the square root of the reduced χ^2. Different approaches to the fitting resulted in extracted cross sections that were outside that estimated uncertainty. For this reason, we estimate an overall uncertainty of 20%, which encompasses different indistinguishable fits. In particular, we have looked at the dependence of the extracted cross section on the ^{10}B thickness for values between 1 and 2μm; for this range of thickness the changes in the extracted cross sections are on the order of 10%, within the quoted 20% fitting uncertainty. Argon has the smallest measured cross section in the presence of a larger absorption cross section; we increased the uncertainty to 30% to account for the range of fits that gave what appear to the eye to be equivalent fits.

In addition to the uncertainties due to statistical and fitting, we have considered the following potential systematic errors: errors due to (1) uncertainty in the length of the gas cell, (2) uncertainty in the neutron velocity (and hence l/v), and (3) the uncertainty in gas pressure. The uncertainty in the size of the gas cell is estimated to be ∼5 mm due to possible bowing of the windows. We estimate the uncertainty in velocity to be due to an uncertainty of 2 cm in the vertical drop.

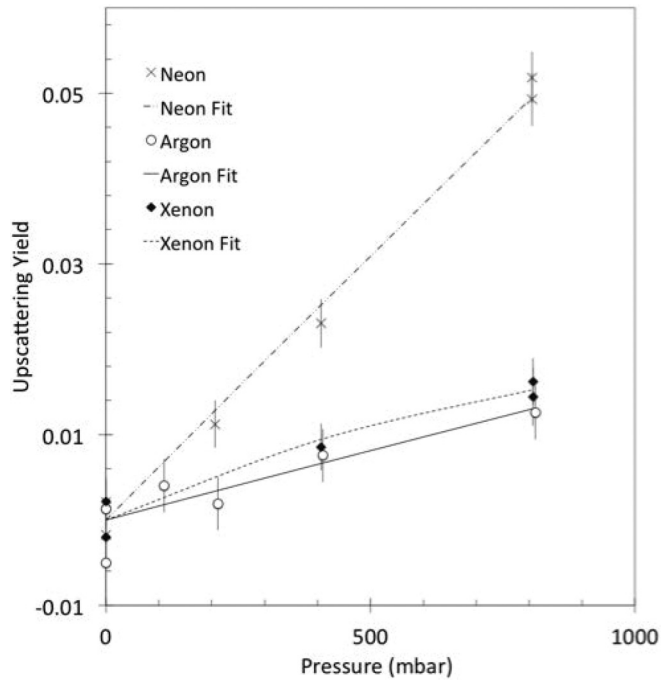

FIG. 11. Upscattering yields from the ^{3}He detector and fits for the polyatomic gas samples.

TABLE I. Upscattering cross sections determined in this paper. Also presented are the absorption cross sections from NIST, the predicted upscattering cross section, and the lifetime correction (for a neutron lifetime of 880 s) of neutrons in the gas calculated in 10^{-6} torr of gas corresponding to the total cross section listed in the table (all cross sections are scaled to 660 cm s). For H_2 and D_2 the measured values from Ref. [7] have been scaled to our energy; for D_2 the measurements with UCNs have been scaled from 20-K D_2 temperature. We estimated the upscattering cross section for air by scaling the results for O_2 and N_2 in Ref. [7] to our energies and adding these according to the partial pressures of these gases in air.

Molecule	σ_{up} (this paper) (barns)	Scaled σ_{up} from Refs. [7] and [10]	σ_{up} (calculated)	$\sigma_{absorption}$(NIST)	σ_{total} (barns)	Correction to $\tau_n(10^{-6}$ torr)
H_2	20 000 (4000)	18 000	16 000	220	20 000	0.3
D_2	3500 (700)	3200	2400	0.35	3500	0.1
Ne	250 (50)		200	13	260	0.0
Ar	70 (20)		40	220	300	0.0
Xe	190 (40)		200	8000	8200	0.1
CF_4	3300 (660)			14	3300	0.1
C_4H_{10}	74 000 (15 000)	96 000	87 000	1100	75 000	1.2
Air	3400 (700)	4600		990	4400	0.1
N_2	3000 (600)		2700	1300	4800	0.1

We have estimated a 1% uncertainty in the gas pressure. The overall systematic uncertainty is 7%—the dominant uncertainty coming from the uncertainty in the length of the gas cell. The cross sections for N_2 and air were measured in a slightly different configuration. These data require different flux normalizations in the direct upscattering data; for this reason only the transmission data are presented Fig. 8.

III. THEORETICAL CONSIDERATIONS

When scattering from a monatomic gas at temperature T, energy is transferred to a cold neutron via atomic recoil, and expressions for the differential and total scattering cross sections for gases have been derived by Zemach and Glauber [19]. In the limit of low incident neutron energy (as is the case for the UCN) these expressions are greatly simplified. For the total upscattering cross section of the UCN, it is convenient to use expressions from Turchin [20],

$$\sigma_{up} = \sigma_{free}\frac{2}{v\sqrt{\pi}}\sqrt{\frac{2kT}{M}} = \sigma_{free}\frac{w}{v}. \tag{11}$$

Here σ_{free} is the total scattering cross section for a free atom at rest [21] (related to the bound cross section σ_b by $\sigma_b = \sigma_{free}(1 + m/M)^2$, v is the initial neutron velocity, and w is the average velocity of gas atoms with mass M. The origin of the $1/v$ behavior of the scattering cross section for gases at low energy is a consequence of the folding of the constant in center-of-mass cross section with the Maxwell-Boltzmann velocities of the gas atoms in a laboratory system. Defining $A = M/m$, the average energy E_{avg} of an upscattered UCN is as follows:

$$E_{avg} = \frac{4AkT}{(A+1)^2}. \tag{12}$$

This follows from the exponential dependence of the differential cross section on the neutron final energy E considered, for example, in the book by Ignatovich [22]. The calculated upscattering cross sections and average energies for the noble gases are shown in Table I for an initial neutron velocity of 660 cm s.

In the case of polyatomic gases, molecular degrees of freedom also contribute to the cross section. To predict the upscattering of the UCN from molecular gases, we must in principle incorporate all translational, rotational, and vibrational motions into a calculation of the dynamical structure function for the gas species in question. In practice, the molecular species measured here are in different regimes with regard to this general prescription, and different approximations and models are therefore necessary.

A rigorous quantum-mechanical treatment of slow neutron scattering from hydrogen and deuterium was performed by Young and Koppel [23]. For gas at room temperature, we can neglect the population or excitation of vibrational modes but must incorporate the first several rotational states. Following Young and Koppel, including only the vibrational ground state and including the six lowest rotational states, we compute σ_{up} for hydrogen and deuterium weighted by their ortho/para concentrations. We also adopt this prescription to calculate the N_2 cross section. Accounting for the differences in mass, scattering length, and spin statistics, we calculate the cross section including the lowest 20 rotational transitions. The values are shown in Table I.

Due to the relatively high mass and high hydrogen content of isobutane (C_4H_{10}), we use the mass-tensor approximation of Sachs and Teller [12] and the monatomic scattering law as applied by Krieger and Nelkin [13]. The mass tensors for the constituent hydrogen atoms can be computed from the principle of reduced moments of inertia and bond structure reported in Ref. [24]. The total upscattering cross section was calculated using an effective mass for constituent H nuclei of approximately 3 amu, which follows from the reduced moments of inertia due to the torsional vibration of CH_3 groups in the molecule. The small rotational constant for rigid-body rotation (i.e., using the principal moments) leads to a much larger effective mass and smaller energy transfers which would be below our neutron detection threshold. It thus

seems reasonable to rely on the reduced moments to determine the average upscattered neutron energy.

We can also estimate the polyatomic cross sections by scaling the known experimental inelastic scattering cross sections for H_2 and C_4H_{10} starting from 2.5 meV (the lowest-energy point in Ref. [7] and using the $1/v$ dependence. The same was performed for air using the N_2 and O_2 data from Ref. [7] and used the result to estimate the cross section for air. For D_2 gas, scattering cross sections have been measured down to UCN energies at 25 K [10], and we scale this to 300 K assuming that the cross section scales as $\sqrt{T}$. The inelastic scattering cross sections for the CF_4 gas in the meV region are unknown. The estimated values for the other gases are shown in Table I. The cross-sectional values are per one atom (noble gases) or per one molecule (others).

IV. CONCLUSIONS

The agreement between the extracted cross sections and the predictions for these gases are quite reasonable for all gases. The calculations for Ar and D_2 are somewhat lower than the measured cross sections. However, the measured upscattering cross section for D_2 is in good agreement with the value scaled from Ref. [10]. This gives us confidence to the use the upscattering cross sections determined from the polyatomic gases to place limits on the contribution of upscattering from these gases to UCN losses in our lifetime measurement.

In order to perform an $\sim$1-s measurement of the lifetime, one would prefer a correction of no more than 0.1 s. This implies a partial pressure of a heavy hydrocarbon, such as C_4H_{10} of no more than 10^{-7} mbars. The requirements for a 0.1-s measurement are even more challenging. However, the most likely contaminants have substantially smaller cross sections, and so this systematic is easily controlled for a 1-s measurement. In future experiments we will measure the upscattering cross section for water vapor. We also plan to repeat the measurements described here with multiple ^{3}He tubes at different pressures so that we can obtain an experimental estimate of the upscattered neutron velocities. In order to fully evaluate the systematics at the level needed for the sub-1-s measurement of the lifetime, it will be necessary to characterize the residual gases in the UCN trap, which should be maintained at a high vacuum.

ACKNOWLEDGMENTS

This material is supported by the LANL LDRD program, the U.S. Department of Energy Office of Science, Office of Nuclear Physics through LANL DOE Grant No. 2015LANLE9BU and North Carolina State University Grant No. DE-FG02-97ER41042, the U.S. National Science Foundation through Indiana University Grants No. PHY-0969490/PHY-1068712, and North Carolina State University grant NSF Grant No. 1307426.

[1] D. J. Salvat *et al.*, Phys. Rev. C **89**, 052501 (2014).
[2] A. Saunders *et al.*, Rev. Sci. Instrum. **84**, 013304 (2013).
[3] S. Arzumanov *et al.*, Phys. Lett. B **483**, 15 (2000).
[4] S. S. Arzumanov, L. N. Bondarenko, V. I. Morozov, Y. N. Panin, and S. M. Chernyavsky, JETP Lett. **95**, 224 (2012).
[5] A. Pichlmaier, V. Varlamov, K. Schreckenbach, and P. Geltenbort, Phys. Lett. B **693**, 221 (2010).
[6] A. Serebrov *et al.*, Phys. Lett. B **605**, 72 (2005).
[7] E. Melkonian, Phys. Rev. **76**, 1750 (1949).
[8] G. L. Squires and A. T. Stewart, Proc. R. Soc. London, Ser. A **230**, 19 (1955).
[9] R. Genin, H. Beil, C. Signarbieux, P. Carlos, R. Joly, and M. Ribrag, J. Phys. Radium **24**, 21 (1963).
[10] F. Atchison *et al.*, Phys. Rev. Lett. **95**, 182502 (2005).
[11] E. P. W. Wigner, Oak Ridge National Laboratory report (unpublished).
[12] R. G. Sachs and E. Teller, Phys. Rev. **60**, 18 (1941).
[13] T. J. Krieger and M. S. Nelkin, Phys. Rev. **106**, 290 (1957).
[14] C. L. Morris *et al.*, Nucl. Instrum. Methods Phys. Res., Sect. A **599**, 248 (2009).
[15] D. J. Salvat *et al.*, Nucl. Instrum. Methods Phys. Res., Sect. A **691**, 109 (2012).
[16] C. L. Morris and A. Roberts, Los Alamos National Laboratory Report No. LA-UR-14-23816, 2014 (unpublished).
[17] V. F. Sears, Neutron News **3**, 26 (1992).
[18] J. F. Briesmeister, Los Alamos National Laboratory Report No. LA-13709-M, version 4C, 2000 (unpublished).
[19] A. C. Zemach and R. J. Glauber, Phys. Rev. **101**, 118 (1956).
[20] V. F. Turchin, *Slow Neutrons* (Israel Program for Scientific Translations, Jerusalem, 1965).
[21] S. F. Mughabghab, *Atlas of Neutron Resonances: Resonance Parameters and Thermal Cross Sections. Z=1–100* (Elsevier, Amsterdam, 2006).
[22] V. K. Ignatovich, *The Physics of Ultracold Neutrons* (Clarendon, Oxford, 1990).
[23] J. A. Young and J. U. Koppel, Phys. Rev. **135**, A603 (1964).
[24] S. S. Chen, R. C. Wilhoit, and B. J. Zwolinski, J. Phys. Chem. Ref. Data **4**, 859 (1975).